https://doi.org/10.5194/amt-2019-426
Preprint. Discussion started: 11 December 2019

Atmospheric Measurement Techniques Discussions

Development of on-site self-calibration and retrieval methods for sky-radiometer observations of precipitable water vapor

Masahiro Momoi[1,2], Rei Kudo[3], Kazuma Aoki[4], Tatsuhiro Mori[5], Kazuhiko Miura[5], Hiroshi Okamoto[1], Hitoshi Irie[1], Yoshinori Shoji[3], Akihiro Uchiyama[6], Osamu Ijima[7], Matsumi Takano[8,7], and Teruyuki Nakajima[9]

[1]Center for Environmental Remote Sensing, Chiba University, Chiba, 263-8522, Japan
[2]Graduate School of Science, Tokyo University of Science, Tokyo, 162-8601, Japan
[3]Meteorological Research Institute, Japan Meteorological Agency, Tsukuba, 305-0052, Japan
[4]Graduate School of Science and Engineering, University of Toyama, Toyama, 930-8555, Japan
[5]Faculty of Science Division I, Tokyo University of Science, Tokyo, 162-8601, Japan
[6]Narional Institute for Environmental Studies, Tsukuba, 305-0053, Japan
[7]Aerological Observatory, Japan Meteorological Agency, Tsukuba, 305-0052, Japan
[8]Osaka Regional Headquarters, Japan Meteorological Agency, Osaka, 540-0008, Japan
[9]Earth Observation Research Center, Japan Aerospace Exploration Agency, Tsukuba, 305-8505, Japan
Correspondence to: Masahiro Momoi (1217641@ed.tus.ac.jp)

https://doi.org/10.5194/amt-2019-426
Preprint. Discussion started: 11 December 2019

Atmospheric Measurement Techniques Discussions

Abstract.

The Prede sky-radiometer, whose aerosol channels are calibrated by on-site measurements (the Improved Langley method), has been used for continuous long-term observation of aerosol properties. However, continuous long-term observation of precipitable water vapor (PWV) by sky-radiometer remain challenge, because the water vapor channel is generally calibrated by the standard Langley method at limited observation sites (*e.g.*, the Mauna Loa Observatory). In this study, we developed SKYMAP, a new onsite self-calibration method for the water vapor channel of the Prede sky-radiometer using diffuse radiances normalized by direct solar irradiance. The SKYMAP algorithm consists of three steps. First, aerosol optical and microphysical properties are retrieved using direct solar irradiances and the normalized diffuse radiances at aerosol channels. The aerosol optical properties at the water vapor channel are interpolated from those at aerosol channels. Second, the transmittance of PWV is retrieved using the diffuse radiance normalized to the direct solar irradiance at the water vapor channel, which does not need the calibration constant. Third, the calibration constant at the water vapor channel is estimated from the transmittance of PWV and aerosol optical properties. Intensive sensitivity tests of SKYMAP using simulated data of the sky-radiometer showed that the calibration constant is retrieved reasonably well for PWV < 2 cm, indicating that SKYMAP can calibrate the water vapor channel on-site in dry conditions. Then SKYMAP was applied to actual measurements in the dry season at two sites (Tsukuba and Chiba, Japan). Because the SKYMAP algorithm is useful for clear-sky and low PWV (< 2 cm) conditions, the water vapor channel was calibrated for the dry season. After determining the calibration constant, PWV is able to be retrieved using direct solar irradiances for the whole year. The retrieved PWV values correspond well to those derived from a Global Navigation Satellite System (GNSS)/Global Positioning System (GPS) receiver, a microwave radiometer, and a AERONET sun-sky radiometer at both sites (correlation coefficient $\gamma > 0.96$), indicating that the Prede sky-radiometer provides both aerosol and PWV data based on its unique on-site calibration methods.

https://doi.org/10.5194/amt-2019-426
Preprint. Discussion started: 11 December 2019

Atmospheric Measurement Techniques Discussions

1 Introduction

The highly variable spatiotemporal distributions of aerosols, clouds, and gases (*e.g.*, water vapor and ozone) still include large uncertainties for the quantitative understanding of the Earth's radiation budget at various spatial and temporal scales. Water vapor is specified as an essential climate variable (ECV) by the World Meteorological Organization (WMO), a critical key parameter that contributes to characterizing Earth's climate and changes in atmospheric temperature (Schmidt *et al.*, 2010). Water vapor absorbs visible radiation and absorbs and emits infrared radiation to heat and cool the Earth and its atmosphere. Atmospheric heating drives the evaporation of sea water, causing an increase in temperature as positive feedback (IPCC, 2013). In addition, the distribution of water vapor controls precipitation amounts and aerosol-cloud interactions (Twomey, 1990). To understand these effects quantitatively, many previous studies have measured columns of water vapor content by using a radiosonde, Global Navigation Satellite System (GNSS)/Global Positioning System (GPS) receiver (Bevis *et al*., 1992), or spectroradiometer (*e.g.*, Fowle, 1912, 1915).

Precipitable water vapor (PWV), which is the total atmospheric water vapor contained in a vertical column, has been estimated from the measurement of direct solar irradiance at the water vapor channel at around 940 nm by sun photometer (Fowle, 1912, 1915; Bruegge *et al.*, 1992; Schmid *et al.*, 1996, 2001; Halthore *et al.*, 1997), SKYNET sky-radiometer (Campanelli *et al.*, 2014, 2018; Uchiyama *et al.*, 2014, 2018a), and AERONET sun-sky photometer (Holben *et al.*, 1998). These previous studies derived PWV from the observed transmittance of water vapor ($\bar{T}_{\mathrm{H2O}}$), assuming $\bar{T}_{\mathrm{H2O}} = e^{-a(m \cdot w)^b}$ (Bruegge *et al*., 1992), where *a* and *b* are adjusting parameters, *m* is the optical air mass, and *w* is PWV. However, there is a known noticeable uncertainty in the estimate of PWV because the adjustment parameters depend on radiometric calibration as well as the vertical profiles of water vapor and temperature. Therefore, Campanelli *et al*. (2014, 2018) developed a practical method for determining the adjusting parameters based on PWV retrieved by a GNSS/GPS receiver or by surface humidity observations.

To estimate PWV using a spectroradiometer, it is necessary to calibrate the water vapor channel. The calibration constant at the water vapor channel can be determined by the Langley method. For example, Uchiyama *et al.* (2014) calibrated the water vapor channel of a sky-radiometer with high accuracy using observations from the Mauna Loa Observatory (3400 m a.s.l.). In the AERONET led by NASA, the AERONET sun-sky radiometer is calibrated every year by lamp calibration and side-by-side comparison with a reference spectroradiometer (Holben *et al.*, 1998). Dedicated effort and cost are required for maintaining accurate long-term calibrations using these methods.

Sky-radiometer POM-02 (Prede, Tokyo, Japan), which is deployed in the international radiation observation network SKYNET, measures solar direct irradiances and angular distributions of diffuse radiances at 11 wavelengths including aerosol, cloud, water vapor, and ozone channels (Takamura and

https://doi.org/10.5194/amt-2019-426
Preprint. Discussion started: 11 December 2019

Atmospheric Measurement Techniques Discussions

Nakajima, 2004; Nakajima *et al.*, 2007). The SKYNET system is capable of long-term and automatic aerosol observation through an on-site self-calibration method, called the Improved Langley (IL) method, which works in turbid atmospheric conditions (Tanaka *et al.*, 1986; Nakajima *et al.*, 1996; Campanelli *et al*., 2004, 2007). However, no improved calibration method has replaced the standard or modified Langley methods for the water vapor channel. In this study, we devised a new method of retrieving PWV using the PWV dependency of the normalized radiance, defined as the ratio of diffuse radiance to direct solar irradiance at the water vapor channel. This method enables us to estimate PWV without the calibration constant, and to perform on-site self-calibration of the water vapor channel. We developed two algorithms, SKYMAP and DSRAD. The SKYMAP algorithm is a new on-site method for self-calibrating the water vapor channel. It retrieves PWV (PWV_{SKYMAP}) from the angular distribution of the normalized radiance at 940 nm and calibrates the water vapor channel. The DSRAD algorithm estimates the PWV (PWV_{DSRAD}) from the calibrated direct solar irradiance at 940 nm. This method does not require adjustment parameters and explicitly uses the filter response function and the vertical profiles of water vapor, temperature and pressure. The SKYMAP and DSRAD algorithms are described in Section 2. We discuss the results of sensitivity tests of the two algorithms using simulation data in Section 3 and apply the algorithms to observational data at two SKYNET sites in Section 4.

2 Methods

In this study, PWV is retrieved using angular distributions of the normalized radiance, which does not require the calibration constant of the sky-radiometer. Section 2.1 shows the normalized radiances and dependencies of the normalized radiance on PWV. Next, we describe two algorithms, the flow and relationships of which are shown in Fig. 1. The SKYMAP algorithm retrieves aerosol optical and microphysical properties and calibrates the water vapor channel by retrieving PWV from the angular distribution of the normalized radiance (Section 2.2). The DSRAD algorithm retrieves PWV from the transmittance derived from the direct solar irradiance at the water vapor channel (Section 2.3).

2.1 Sky-radiometer measurements and relation between normalized radiances and the PWV

We explain normalized radiance in Section 2.1.1 and the theoretical relationship between normalized radiances and PWV in Section 2.1.2.

2.1.1 Sky-radiometer measurements

The direct solar irradiance (F) and angular distribution of diffuse radiance (L) are measured at 11 wavelengths, including aerosol (λ = 340, 380, 400, 500, 675, 870, and 1020 nm), cloud (1627 and 2200 nm), water vapor (940 nm), and ozone (315 nm) channels. L is measured in the almucantar and principal planes (Fig. 2). The angular distribution of L is measured at scattering angles Θ = 2°, 3°, 4°, 5°,

https://doi.org/10.5194/amt-2019-426
Preprint. Discussion started: 11 December 2019

Atmospheric Measurement Techniques Discussions

7°, 10°, 15°, 20°, 25°, 30°, 40°, 50°, 60°, 70°, 80°, 90°, 100°, 110°, 120°, 130°, 140°, 150°, and 160° in the almucantar and principal planes, every 10 min. Aerosol channels are calibrated with the IL method using the normalized radiance at $\Theta < 30°$. F and $L(\Theta \geqq 4°)$ at aerosol and water vapor channels are used in this study.

The direct solar irradiance at the bottom of the atmosphere (BOA) at the solar zenith angle (SZA) θ_0 and the solar azimuth angle ϕ_0 is derived from

$$F(\lambda) = \frac{F_0}{d^2} \exp\left(-m_0 \tau(\lambda)\right) \quad (1),$$

where F_0 is the calibration constant, which is the sensor output current of the direct solar irradiance at the top of the atmosphere (TOA) when the distance between Earth and the sun is 1 AU; d is the distance between Earth and the sun (AU); λ is the wavelength; τ is the total optical thickness; and m_0 is optical air mass, represented as $m_0 = 1/\cos\theta_0$ in the plane-parallel nonrefractive atmosphere. In clear-sky conditions, the total optical thickness consists of aerosol scattering/absorption, Rayleigh scattering, gas absorption and integrated from BOA to TOA. Assuming a narrow spectral band filter response function, the normalized radiance (R) which is the ratio of L to F at the zenith angle (θ) and the azimuth angle (ϕ) is obtained from the radiative transfer equation:

$$R(\Theta,\lambda) = \frac{L(\Theta,\lambda)}{F(\lambda) m_0 \Delta\Omega} = \int_0^{\tau(\lambda)} \exp\left[(\tau - \tau')\left(\frac{1}{\mu_0} - \frac{1}{\mu}\right)\right] \omega'(\lambda,\tau') P'(\Theta,\lambda,\tau') d\tau' + Q(\Theta,\lambda) \quad (2),$$

where $P'(\Theta,\lambda,\tau')$ and $\omega'(\lambda,\tau')$ are, the total phase function and the total single scattering albedo, respectively, at the altitude $\tau = \tau'$, $\Delta\Omega$ is the solid view angle (or field of view); Q is the multiple scattering contribution; and

$$\cos\Theta = \cos\theta\cos\theta_0 + \sin\theta\sin\theta_0\cos(\phi - \phi_0) \quad (3),$$
$$\mu = \cos\theta\,;\mu_0 = \cos\theta_0$$

Noted that F_0 is cancelled by the normalization. In the second term of Eq. (2), the solid view angle of each wavelength can be retrieved from the angular distribution around the solar disk (Nakajima *et al.*, 1996; Boi *et al.*, 1999; Uchiyama *et al.*, 2018b). Eq. (2) can be simplified in the almucantar plane due to $\theta = \theta_0$:

$$R(\Theta,\lambda) = \int_0^{\tau(\lambda)} \omega'(\lambda,\tau') P'(\Theta,\lambda,\tau') d\tau' + Q(\Theta,\lambda) = \omega(\lambda)\tau(\lambda)P(\Theta,\lambda) + Q(\Theta,\lambda) \quad (4),$$

https://doi.org/10.5194/amt-2019-426
Preprint. Discussion started: 11 December 2019

Atmospheric Measurement Techniques Discussions

where $P(\Theta,\lambda)$ and ω are the total phase function and the total single scattering albedo, respectively. In contrast, normalized radiances in the principal plane can be described simply, similar to Eq. (4), if we assume that the atmosphere is a single layer:

$$R(\Theta,\lambda) = \frac{\mu_0^2}{\mu_0-\mu}\omega(\lambda)P(\Theta,\lambda)\left[1-\exp\left(\frac{\tau(\lambda)}{\mu_0}-\frac{\tau(\lambda)}{\mu}\right)\right]+Q(\Theta,\lambda) \qquad (5).$$

Noted that real atmosphere is not a single layer (Torres *et al.*, 2014).

2.1.2 The relationship between normalized radiances at the water vapor channel and PWV

We examined the sensitivity of *R* in the two observation planes to PWV, aerosol optical properties, and aerosol vertical profiles by simulating *R*. Figure 3 shows the dependencies of *R* on PWV for continental average aerosol (Table 1) with aerosol optical thicknesses of 0.02 and 0.20 at an SZA of 70° in the almucantar plane. *R* decreases with increasing PWV, and the aerosol optical thickness does not affect this relationship. This suggests that PWV can be estimated from the normalized angular distribution, which is the angular distribution of *R*, without the calibration constant. The dependencies of *R* on PWV cannot be observed in the radiative transfer using single scattering approximation in the almucantar plane. The first term of Eq. (4) is the normalized single scattering contribution and includes only the influences of aerosol and Rayleigh scattering. Noted that this is true only for *R*, and not for *L*, because total optical thickness contributes to single scattering approximation of *L*. However, the second term for the multiple scattering includes the influence of water vapor absorption and creates the dependencies of *R* on PWV. Figure 3 shows that the dependency of *R* on PWV at the forward scattering angles is not strong, but *R* at the backward scattering angles between 90° and 120° changes drastically with PWV. The range of the scattering angle for *R* is an important factor.

Figure 4 illustrates the dependency of *R* on PWV for different observation planes. The simulation was conducted for transported dust aerosol (Table 1) with an aerosol optical thickness of 0.06 at an SZA of 70° in the almucantar and principal planes. The dependency of *R* on PWV was found in both observation planes. Although the dependency of *R* on PWV in the almucantar plane is strong at the backward scattering angles, that in the principal plane is strong at scattering angles between 60° and 90°. *R* in the principal plane is more sensitive to PWV than *R* in the almucantar plane because the normalized single scattering contribution in Eq. (5) includes not only Rayleigh and aerosol scattering but also gas absorption.

In theory, the maximum scattering angle of the principal plane is θ_0 + 90° and that of the almucantar plane is $2\theta_0$. When the SZA is small, the principal plane has a broader scattering angle range than the almucantar plane. Therefore, the principal plane is more advantageous for PWV retrieval. Figure 5 is the same as Fig. 4 but for an SZA of 30°. Because the maximum scattering angle of the

https://doi.org/10.5194/amt-2019-426
Preprint. Discussion started: 11 December 2019

Atmospheric Measurement Techniques Discussions

principal plane is obviously larger than that of the almucantar plane, PWV retrieval using the principal plane is more effective compared to that using the almucantar plane.

R in the principal plane is affected by the aerosol vertical profile, but this influence can be ignored for *R* in the almucantar plane (Torres *et al*., 2014). Figure 6 shows the normalized angular distribution in the two observation planes for the different heights of the transported dust layer. It is obvious that the normalized angular distribution in the principal plane is sensitive to the aerosol vertical profile. Consequently, the principal plane is useful for retrieving PWV when the aerosol vertical profile is known, but the almucantar plane is better when the aerosol vertical profile is not known. In this study, we used the normalized angular distribution in the almucantar plane because the aerosol vertical profile was not known. The influence of SZA on the retrieval of PWV is examined in Section 3.

2.2 SKYMAP algorithm

The SKYMAP algorithm consists of three steps (Fig. 7). First, aerosol optical and microphysical properties are retrieved from *F* and normalized angular distributions at aerosol channels. Second, aerosol optical properties at the water vapor channel are interpolated from those at aerosol channels. PWV is retrieved from the normalized angular distribution at the water vapor channel. Third, the calibration constant at the water vapor channel is estimated from PWV and the aerosol optical properties.

2.2.1 Step 1: Retrieval of aerosol optical and microphysical properties

Aerosol optical and microphysical properties are estimated from sky-radiometer measurements at aerosol channels using normalized angular distributions and transmittance of the total extinction $T = \frac{I_{\mathrm{dir}}}{F_0}$ with an optimal estimation method similar to the AERONET and SKYNET retrievals (Dubovik and King, 2000; Dubovik *et al.*, 2006; Kobayashi *et al.*, 2006; Hashimoto *et al.*, 2012; Kudo *et al.*, 2016). Estimated optical and microphysical properties are the real and imaginary parts of the refractive index at aerosol channels (340, 380, 400, 500, 675, 870, 1020 nm), the volume size distribution, and the volume ratio of non-spherical particles to total particles in coarse mode. Hereafter, these are referred to as aerosol parameters.

In step 1, we construct the forward model to calculate the sky-radiometer measurements from the aerosol parameters. We assume that the aerosol volume size distribution in the radius range from 0.02 to 20.0 μm consists of 20-modal lognormal volume size spectra as illustrated in Fig. 8:

$$\frac{\mathrm{d}V(r)}{\mathrm{d}\ln r} = \sum_{i=1}^{20} C_i \exp\left[-\frac{1}{2}\left(\frac{\ln r - \ln r_i}{s}\right)^2\right] \quad (6),$$

$$\ln r_i = \ln(0.02\mu\mathrm{m}) + \frac{2i-1}{2}\ln \Delta r \quad (7),$$

https://doi.org/10.5194/amt-2019-426
Preprint. Discussion started: 11 December 2019

Atmospheric Measurement Techniques Discussions

$$s \equiv \frac{\ln \Delta r}{1.65} \qquad (8),$$

$$\ln \Delta r \equiv \frac{1}{20}(\ln(20\mu m) - \ln(0.02\mu m)) = \frac{3}{20}\ln 10 \qquad (9),$$

where C_i, r_i, and s are the volume, radius, and width of each lognormal function, respectively. We can separate the size distribution into fine and coarse modes by giving the boundary radius r_b, which is obtained as the local minimum. Furthermore, we separate coarse mode into spherical and non-spherical particles:

$$\frac{\mathrm{d}V(r)}{\mathrm{dln}r} = \frac{\mathrm{d}V_\mathrm{f}(r)}{\mathrm{dln}r} + (1-\delta)\frac{\mathrm{d}V_\mathrm{c}(r)}{\mathrm{dln}r} + \delta\frac{\mathrm{d}V_\mathrm{c}(r)}{\mathrm{dln}r} \qquad (10),$$

where $\frac{\mathrm{d}V_\mathrm{f}(r)}{\mathrm{dln}r}$ is fine mode, $\frac{\mathrm{d}V_\mathrm{c}(r)}{\mathrm{dln}r}$ is coarse mode, and δ is the fraction of the non-spherical particles in coarse mode (Fig. 8). The aerosol optical properties are calculated from the size distribution and refractive index, similar to methods of Kudo *et al*. (2016) and Dubovik *et al.* (2006), as follows:

$$\tau_{\mathrm{ext/sca}}(\lambda) = \sum_k \frac{dV_\mathrm{f}(r_k)}{d\ln r} K^\mathrm{S}_{\mathrm{ext/sca}}(\lambda, n, k, r_k) + \sum_k (1-\gamma)\frac{dV_\mathrm{c}(r_k)}{d\ln r} K^\mathrm{S}_{\mathrm{ext/sca}}(\lambda, n, k, r_k) + \sum_k \gamma \frac{dV_\mathrm{c}(r_k)}{d\ln r} K^\mathrm{NS}_{\mathrm{ext/sca}}(\lambda, n, k, r_k) \qquad (11)$$

$$\tau_{\mathrm{sca}}(\lambda) P_{ii}(\Theta, \lambda) = \sum_k \frac{dV_\mathrm{f}(r_k)}{d\ln r} K^\mathrm{S}_{ii}(\Theta, \lambda, n, k, r_k) + \sum_k (1-\gamma)\frac{dV_\mathrm{c}(r_k)}{d\ln r} K^\mathrm{S}_{ii}(\Theta, \lambda, n, k, r_k) + \sum_k \gamma \frac{dV_\mathrm{c}(r_k)}{d\ln r} K^\mathrm{NS}_{ii}(\Theta, \lambda, n, k, r_k) \qquad (12)$$

where $\tau_{\mathrm{ext/sca}}(\lambda)$ denotes the optical thickness of extinction and scattering, and $\tau_{\mathrm{sca}}(\lambda)P_{ii}(\Theta, \lambda)$denotes the directional scattering corresponding to the scattering matrix elements $P_{ii}(\Theta, \lambda)$. K^S and K^NS are the kernels of extinction and scattering properties for spherical and non-spherical particles, respectively. n and k are the real and imaginary parts of the refractive index, respectively. We use randomly oriented spheroids as non-spherical particles and use the kernels developed by Dubovik *et al.* (2006).

We compute normalized angular distributions and transmittances of the extinction, using the radiative transfer model RSTAR (Nakajima and Tanaka, 1986, 1988). The model atmosphere is divided by 18 boundary layers at 0, 1, 2, 3, 4, 5, 6, 7, 8, 9, 10, 15, 20, 30, 40, 50, 70, and 120 km. Atmospheric vertical profiles of temperature and pressure are obtained from NCEP/NCAR Reanalysis 1 data. The absorption coefficients of H_2O, CO_2, O_3, N_2O, CO, CH_4, and O_2 are calculated by the correlated *k*-distribution method from the data table of Sekiguchi and Nakajima (2008).

https://doi.org/10.5194/amt-2019-426
Preprint. Discussion started: 11 December 2019

Atmospheric Measurement Techniques Discussions

The aerosol parameters for the best fit to all measurements (normalized angular distributions and transmittances at aerosol channels) and *a priori* information are obtained by minimizing the following cost function,

$$f(\boldsymbol{x}) = \frac{1}{2}\left(\boldsymbol{y}^{\text{meas}} - \boldsymbol{y}(\boldsymbol{x})\right)^T (\boldsymbol{W}^2)^{-1}\left(\boldsymbol{y}^{\text{meas}} - \boldsymbol{y}(\boldsymbol{x})\right) + \frac{1}{2}\left(\boldsymbol{y}_a(x)\right)^T (\boldsymbol{W}_a^2)^{-1}\left(\boldsymbol{y}_a(x)\right) \quad (13),$$

where vector $\boldsymbol{y}^{\text{meas}}$ describes the measurements (normalized radiances R^{meas} and transmittances of total extinction T^{meas} at aerosol channels), vector $\boldsymbol{x}$ describes the aforementioned aerosol parameters —$n(\lambda)$, $k(\lambda)$, C_i, and δ— to be estimated, vector $\boldsymbol{y}(\boldsymbol{x})$ comprises the values corresponding to $\boldsymbol{y}^{\text{meas}}$ calculated from $\boldsymbol{x}$ by the forward model (R^{ret} and T^{ret}), and matrix $\boldsymbol{W}^2$ is the covariance matrix of $\boldsymbol{y}$ and is assumed to be diagonal. The diagonal elements of $\boldsymbol{W}$ are the standard errors in the measurements. We set their values at 0.02 for T^{meas}, and 10% for R^{meas}.

To reduce the effects of observational error on retrieval and to conduct stable analyses, Dubovik and King (2000) considered restricting the spectral variability of the refractive index by limiting the length of the derivatives of the refractive index with respect to the wavelength and the volume size distribution. They considered this *a priori* smoothness constraint as being of the same nature as a measurement and incorporated the smoothness constraint into their retrieval scheme. We also consider the smoothness constraints in this study. The second term of Eq. (13) consists of *a priori* information on the wavelength dependencies of the refractive index, aerosol optical thickness, and smoothness of the volume spectrum, which is described as

$$\boldsymbol{y}_a(x) = \left(\boldsymbol{y}_a^{\text{Re}}, \boldsymbol{y}_a^{\text{Im}}, \boldsymbol{y}_a^{\text{Sca}}, \boldsymbol{y}_a^{\text{Abs}}, \boldsymbol{y}_a^{\text{Vol}}\right)^T \quad (14),$$

where vectors $\boldsymbol{y}_a^{\text{Re}}$, $\boldsymbol{y}_a^{\text{Im}}$, $\boldsymbol{y}_a^{\text{Sca}}$, $\boldsymbol{y}_a^{\text{Abs}}$, and $\boldsymbol{y}_a^{\text{Vol}}$ are *a priori* information on the wavelength dependencies of the refractive index (real and imaginary parts), aerosol optical thickness (scattering and absorption parts), and smoothness of the volume spectrum, respectively. The matrix $\boldsymbol{W}_a{}^2$ in Eq. (13) is the covariance matrix for determining the strengths of the constrains.

We adapt the smoothness constraint of the second derivatives for the real and imaginary parts of the refractive index. The second derivatives are defined as

$$y_a^{\text{Re}(i)}(\boldsymbol{x}) = \left(\frac{\ln n(\lambda_i) - \ln n(\lambda_{i+1})}{\ln \lambda_i - \ln \lambda_{i+1}} - \frac{\ln n(\lambda_{i+1}) - \ln n(\lambda_{i+2})}{\ln \lambda_{i+1} - \ln \lambda_{i+2}}\right) \quad (15),$$

$$y_a^{\text{Im}(i)}(\boldsymbol{x}) = \left(\frac{\ln k(\lambda_i) - \ln k(\lambda_{i+1})}{\ln \lambda_i - \ln \lambda_{i+1}} - \frac{\ln k(\lambda_{i+1}) - \ln k(\lambda_{i+2})}{\ln \lambda_{i+1} - \ln \lambda_{i+2}}\right) \quad (16),$$

$$(i = 1, \cdots, N_w - 2),$$

https://doi.org/10.5194/amt-2019-426
Preprint. Discussion started: 11 December 2019

Atmospheric Measurement Techniques Discussions

where $y_a^{\mathrm{Re}(i)}$ and $y_a^{\mathrm{Im}(i)}$ are the i-th elements of the vectors $\boldsymbol{y}_a^{\mathrm{Re}}$ and $\boldsymbol{y}_a^{\mathrm{Im}}$, respectively. N_{w} is the number of wavelengths. The values entered into the weight matrix $\boldsymbol{W_a}$ are 0.2 for the real part and 1.25 for the imaginary part. These values are adopted from Dubovik and King (2000). Furthermore, we introduce the smoothness constraints to the spectral distributions of the scattering and absorption parts of the aerosol optical thickness by

$$y_a^{\mathrm{Sca}(i)}(\boldsymbol{x}) = \left(\frac{\ln \tau_{sca}(\lambda_i) - \ln \tau_{sca}(\lambda_{i+1})}{\ln \lambda_i - \ln \lambda_{i+1}} - \frac{\ln \tau_{sca}(\lambda_{i+1}) - \ln \tau_{sca}(\lambda_{i+2})}{\ln \lambda_{i+1} - \ln \lambda_{i+2}}\right) \quad (17),$$

$$y_a^{\mathrm{Abs}(i)}(\boldsymbol{x}) = \left(\frac{\ln \tau_{abs}(\lambda_i) - \ln \tau_{abs}(\lambda_{i+1})}{\ln \lambda_i - \ln \lambda_{i+1}} - \frac{\ln \tau_{abs}(\lambda_{i+1}) - \ln \tau_{abs}(\lambda_{i+2})}{\ln \lambda_{i+1} - \ln \lambda_{i+2}}\right) \quad (18),$$
$$(i = 1, \cdots, N_w - 2),$$

where $y_a^{\mathrm{Sca}(i)}$ and $y_a^{\mathrm{Abs}(i)}$ are the i-th elements of the vectors $\boldsymbol{y}_a^{\mathrm{Sca}}$ and $\boldsymbol{y}_a^{\mathrm{Abs}}$, respectively. The value entered in the weight matrix $\boldsymbol{W_a}$ is 2.5 for both the scattering and absorption parts of the aerosol optical thickness. To stabilize the estimation of the volume size distribution, we introduce the smoothness constraint for the adjacent volume size spectrum C_i, as:

$$y_a^{\mathrm{Vol}(i)}(\boldsymbol{x}) = (\ln C_{i-1} - \ln C_i) - (\ln C_i - \ln C_{i+1}) \quad (19),$$
$$(i = 1, \cdots, 20),$$

$$C_0 = 0.01 \times \min\{C_i | i = 1, \cdots, 20\},\ C_{21} = 0.01 \times \min\{C_i | r_i > r_b, i = 1, \cdots, 20\}.$$

where $y_a^{\mathrm{Vol}(i)}$ is the i-th element of the vector $\boldsymbol{y}_a^{\mathrm{Vol}}$. The small values of C_0 and C_{21} at r_0 and r_{21} are given to prevent both ends of the size distribution (C_1 and C_{20}) from being abnormal values because the solar direct irradiances and diffuse radiances do not have sufficient information to estimate the size distribution of both small (r < 0.1 μm) and large particles (r > 7 μm; Dubovik *et al.*, 2000). Note that r_0 and r_{21} satisfy Eq. (7). The value entered in the weight matrix $\boldsymbol{W_a}$ is 1.6 for the smoothness constraint of the size distribution.

We minimize $f(\boldsymbol{x})$ of Eq. (13) using the algorithm developed in Kudo *et al*. (2016), which is based on the Gauss-Newton method and the logarithmic transformations of $\boldsymbol{x}$ and $\boldsymbol{y}$. Finally, the aerosol optical properties from aerosol channels are obtained from $\boldsymbol{x}$ using Eqs. (11) and (12).

https://doi.org/10.5194/amt-2019-426
Preprint. Discussion started: 11 December 2019

Atmospheric Measurement Techniques Discussions

2.2.2 Step 2: Retrieval of PWV

We estimate PWV by the following procedure. The aerosol volume size distribution is obtained from step 1, and the refractive index at 940 nm is calculated from those at 870 and 1020 nm by linear interpolation in the log-log plane. Using the size distribution and the interpolated refractive index, we can compute the aerosol optical properties and the normalized angular distribution at the water vapor channel using the forward model described in Section 2.2.1. We retrieve PWV by minimizing the following cost function:

$$f(\boldsymbol{x}) = \frac{1}{2}\left(\boldsymbol{y}^{\text{meas}} - \boldsymbol{y}(\boldsymbol{x})\right)^{T}(\boldsymbol{W}^{2})^{-1}\left(\boldsymbol{y}^{\text{meas}} - \boldsymbol{y}(\boldsymbol{x})\right) \quad (20),$$

where the component of vector $\boldsymbol{x}$ is PWV, vectors $\boldsymbol{y}^{\text{meas}}$ and $\boldsymbol{y}(\boldsymbol{x})$ are the normalized angular distribution in the range of 4° to 160°, matrix $\boldsymbol{W}^2$ is assumed to be diagonal, and the values of the diagonal matrix $\boldsymbol{W}$ are assumed to be 10%. The cost function is minimized by the Gauss-Newton method. Note that this process does not require calibration constants of the sky-radiometer, because we use the normalized angular distribution (Eq. [4]) to obtain PWV instead of using the direct solar irradiance (Eq. [1]).

2.2.3 Step 3: Retrieval of the calibration constant of the water vapor channel

F_0 at the water vapor channel can be obtained from the observed F and the band average transmittance $\bar{T}_{\text{H2O}}$ converted from PWV in step 2 as follows:

$$F_0 = \frac{Fd^2 e^{m\cdot(\tau_R+\tau_a)}}{\bar{T}_{\text{H2O}}} \quad (21),$$

where τ_R and τ_a are Rayleigh scattering and aerosol optical thicknesses, respectively. The band average transmittance can be written as

$$\bar{T}_{\text{H2O}} = \frac{1}{\Delta\lambda}\int_{\Delta\lambda}\Phi(\lambda)T_{\text{H2O}}(\lambda)d\lambda = \frac{1}{\Delta\lambda}\int_{\Delta\lambda}\Phi(\lambda)\exp\left(-m_{\text{H2O}}(\theta)\int_0^z \sigma_{\text{H2O}}(g_w(z),K(z),\lambda)dz\right)d\lambda \quad (22),$$

$$w = \int_0^z g_w(z)dz \quad (23),$$

where $\Phi(\lambda)$ is the filter response function, $\Delta\lambda$ is the bandwidth of the filter response function, T_{H2O} is the transmittance of water vapor at wavelength λ, $m_{\text{H2O}}(\theta)$ is the optical air mass, g_w is the mass mixing ratio, K is temperature, σ_{H2O} is the absorption coefficient at altitude z, and w is PWV. Eq. (22) is discretized by

https://doi.org/10.5194/amt-2019-426
Preprint. Discussion started: 11 December 2019

Atmospheric Measurement Techniques Discussions

$$\bar{T}_{\mathrm{H2O}} = \frac{1}{\Delta\lambda}\sum_i^{N_s} \Phi_i \int_{\Delta\lambda_i} \exp\left(-m_{\mathrm{H2O}}(\theta) \int_0^z \sigma_{\mathrm{H2O}}(g_w(z), K(z), \lambda) dz\right) d\lambda \quad (24)$$

where Φ_i is the stepwise filter response function, $\Delta\lambda_i$ is the sub-bandwidth of the filter response function, and N_s is the number of sub-bands. We calculate the absorption coefficients at each wavelength by the correlated *k*-distribution (Sekiguchi and Nakajima, 2008) using the vertical profiles of temperature, pressure, and specific humidity in the NCEP/NCAR Reanalysis 1 data.

We can calculate a value for F_0 from a data set of the normalized angular distribution. Therefore, for example, the time series of F_0 in a day is obtained from the daily measurements of the sky-radiometer. The mean value of the calibration constant at the water vapor channel is determined by the robust statistical method with Huber's M-estimation:

$$\ln \bar{F}_0 = \sum w_{\mathrm{H}} \cdot \ln F_0 \quad (25),$$

$$w_{\mathrm{H}} = \begin{cases} 1 & (|\ln \bar{F}_0 - \ln F_0| \le 0.03) \\ \frac{0.03}{|\ln \bar{F}_0 - \ln F_0|} & (|\ln \bar{F}_0 - \ln F_0| > 0.03) \end{cases} \quad (26),$$

where $\bar{F}_0$ is the mean calibration constant, F_0 is the calibration constant at a specific time, and w_{H} is Huber's weight function.

2.2.4 Cloud screening using the smoothness criteria of the angular distributions (SCAD method)

The SKYMAP algorithm can only be applied to measurements under clear-sky conditions. We estimated clear-sky conditions from two indexes calculated from sky-radiometer measurements. Index 1 is a value for diffuse radiances near the sun. If clouds pass over the sun, index 1 has large temporal variation. Index 2 is a value for the normalized angular distribution. If clouds are detected on the scanning plane of the sky-radiometer, the normalized angular distribution has large variation. Index 1 is defined as follows. First, the mean normalized radiance near the sun is calculated by

$$R_{\mathrm{near}}(t) = \frac{1}{N}\sum_{i=1}^{N} R(\Theta_i, t),\ \Theta \le 10^{\mathrm{o}} \quad (27),$$

where N is the number of measurements, and R is the normalized radiance at time t, scattering angle Θ, and wavelength 500 nm. Next, the running mean of the time series of $R_{\mathrm{near}}(t)$ with a window of three consecutive data points is calculated as $R_{\mathrm{near,mean}}(t)$. Index 1 is defined as the deviation of $R_{\mathrm{near}}(t)$ from $R_{\mathrm{near,mean}}(t)$,

https://doi.org/10.5194/amt-2019-426
Preprint. Discussion started: 11 December 2019

Atmospheric Measurement Techniques Discussions

$$R_{\mathrm{near,dev}}(t) = \left|R_{\mathrm{near}}(t) - R_{\mathrm{near,mean}}(t)\right| / R_{\mathrm{near,mean}}(t) \quad (28).$$

Index 2 is the deviation of normalized angular distributions far from the sun and is defined as

$$R_{\mathrm{far,dev}}(t) = \sigma\left(\frac{R(\Theta,t) - R_{\mathrm{far,mean}}(\Theta,t)}{R_{\mathrm{far,mean}}(\Theta,t)}\right), \Theta > 10 \text{ degree} \quad (29),$$

where $R_{\mathrm{far,mean}}(\Theta,t)$ is the running mean of $R(\Theta_i,t)$ with a window of three consecutive data points, and $\sigma(\mathbf{X})$ is the standard deviation of data set $\mathbf{X}$. We judged clear-sky conditions, when two indexes 1 and 2 were both below two thresholds (0.1 and 0.2, respectively). We determined the thresholds by comparing the images of the whole-sky camera and the time series of the surface solar radiation observed by the pyranometer. Figure 9 is an example of the results for observations on January 6, 2014 in Tsukuba. Clear-sky conditions continued until 12:30, and then clouds passed over the sky until 15:00. Subsequently, there were clouds near the horizon, but the sky was almost clear. Our algorithm worked well, and cloudy scenes were eliminated. However, the cloudy conditions from 14:00 to 15:00 were misjudged, because the sky-radiometer observes only a part of the whole sky. The decline in the surface solar radiation around 9:00 was due to wiping of the glass dome of the pyranometer to keep the dome clean.

The method was applied to measurements from 2013 to 2014 at the Meteorological Research Institute, Japan Meteorological Agency (MRI, JMA), in Tsukuba. The results were validated using visual observation of the amount of clouds in the Aerological Observatory of the JMA. Table 2 shows the validation results of this method. We defined “clear sky” as cloud cover < 1 and “cloud affected” as cloud cover > 2. In less than 17% of cases a cloudy sky was misjudged as a clear sky. The sky-radiometer observes only a part of the whole sky, but our algorithm showed good results.

2.3 Estimation of PWV from direct solar irradiance (DSRAD algorithm)

The sky-radiometer observes the angular distribution of L every 10 min but observes the direct solar irradiance every 1 min. Once the calibration constant is determined by the SKYMAP algorithm, we can estimate PWV from the direct solar irradiance. The DSRAD algorithm computes the aerosol optical thickness, and PWV from the direct solar irradiances at the aerosol and water vapor channels. Table 3 shows the references of the DSRAD algorithm. This algorithm consists of two steps. First, aerosol optical thicknesses at aerosol channels are calculated using direct solar irradiances. The aerosol optical thickness at the water vapor channel is interpolated from the aerosol optical thicknesses at 870 and 1020 nm by line regression. Second, the band mean transmittance of the water vapor, $\bar{T}_{\mathrm{H2O}}^{\mathrm{meas}}$, is calculated from the calibrated direct solar irradiance. PWV is retrieved using the formula,

https://doi.org/10.5194/amt-2019-426
Preprint. Discussion started: 11 December 2019

Atmospheric Measurement Techniques Discussions

$$\bar{T}_{\mathrm{H2O}}^{\mathrm{meas}} - \frac{1}{\Delta\lambda}\sum_{i}^{N_s}\Phi_i \int_{\Delta\lambda_i} \exp\left(-m_{\mathrm{H2O}}(\theta)\int_0^z \sigma_{\mathrm{H2O}}(g_w(z), K(z), \lambda)dz\right) d\lambda = 0 \qquad (30)$$

where m_{H2O} is the optical air mass calculated by Gueymard (2001). Eq. (30) is solved using the Newton–Raphson method.

To ensure the quality of the data and avoid cloud contamination, we adopt the method of Smirnov *et al*. (2000) with two main differences, similar to Estellés *et al*. (2012). First, an aerosol optical thickness at 500 nm > 2 is considered cloud-affected data. Second, the triplet of the aerosol optical thickness in Smirnov *et al*. (2000) is built from 1 min instead of 30 s.

3 Sensitivity tests using simulated data

We conducted sensitivity tests using simulated data to evaluate SKYMAP algorithm steps 1 and 2 (Figs. 7a and 7b). The simulation was conducted using two aerosol types based on those used by Kudo *et al*. (2016): the continental average, and the continental average + transported dust in the upper atmosphere (Table 1). The continental average consisted of water-soluble particles, soot particles, and insoluble particles (Hess *et al*., 1999). Transported dust was defined as the mineral-transported component from Hess *et al*. (1999). The sensitivity test was conducted with sky radiances in the almucantar plane for aerosol optical thicknesses of 0.02, 0.06, and 0.20 at 940 nm; PWV of 0.0, 0.5, 1.0, 1.5, 2.0, 2.5, 3.0, 3.5, 4.0, 4.5, and 5.0 cm; SZA = 30°, 50°, and 70°.

Figure 10 illustrates the retrieval results from the simulated data for the continental average aerosol with aerosol optical thicknesses of 0.02, 0.06, and 0.20 at 940 nm. The retrievals of the size distribution, aerosol optical thickness, and PWV corresponded with their input values when the input of PWV was <2 cm. This was seen regardless of the magnitude of the aerosol optical thickness. When the input of PWV was >2 cm, the size distribution, scattering and absorption optical thickness were retrieved well, but PWV was underestimated. When PWV was >2 cm, the normalized angular distribution was insensitive to PWV (Fig. 3). Figure 11 illustrates the retrieval results from the simulated data for the transported dust aerosol with aerosol optical thicknesses of 0.02, 0.06 and 0.20 at 940 nm. The scattering and absorption optical thickness were retrieved well. The size distribution of fine mode was slightly overestimated. Retrieval errors increased with increasing aerosol optical thickness because the near-infrared wavelength was strongly affected by the retrieval of coarse mode particles.

When the input of PWV is <2 cm, the SKYMAP retrieved PWV very well within an error of 0.5 cm, regardless of the aerosol optical thickness or the aerosol type. The scattering and absorption parts of aerosol optical thickness were also estimated very well within ± 0.01 in all conditions. Present

https://doi.org/10.5194/amt-2019-426
Preprint. Discussion started: 11 December 2019


Atmospheric Measurement Techniques Discussions

sensitivity tests suggest the design of a sky-radiometer calibration program as follows: to determine the calibration constant of the water vapor channel in dry days/seasons with PWV <2 cm, and to obtain PWV from solar irradiance data throughout the year, as illustrated in Fig. 1.

4 Application to observational data

We applied our methods to SKYNET sky-radiometer data in Tsukuba and Chiba. The results were compared to PWV observed by instruments other than the sky-radiometer. Aerosol channels of the sky-radiometer were calibrated by the IL method with SKYRAD.pack version 4.2 (Nakajima *et al*., 1996; Campanelli *et al*., 2004, 2007), and the solid view angles of all channels were calibrated by on-site methods (Nakajima *et al*., 1996; Boi *et al*., 1999; Uchiyama *et al*., 2018b).

4.1 Observation at Tsukuba

In Tsukuba, the sky-radiometer (S/N PS1202091) is installed at the MRI (36.05°N, 140.12°E). We used data from 2013 and 2014. The water vapor channel of PS1202091 was calibrated each winter by side-by-side comparison with the reference sky-radiometer, which was calibrated by the Langley method at the NOAA Mauna Loa Observatory (Uchiyama *et al.*, 2014). PWV was also observed using a GNSS/GPS receiver (Shoji, 2013) at Ami station (No. 0584; 36.03°N, 140.20°E), approximately 7.5 km east-southeast of the MRI.

The calibration constant of the water vapor channel was determined for each month (Figs. 12a and 13a). To obtain the correct value, we used retrieval results with PWV_{SKYMAP} < 2 cm and sufficiently small cost functions (Eqs. [13) and [20]). The annual mean values for 2013 and 2014 were 1.886×10^{-4} A and 2.212×10^{-4} A, respectively. Because the lens at the visible and near-infrared wavelengths was replaced in December 2013, the calibration constants at these wavelengths changed drastically (annual mean value: + 17.2 % from 2013 to 2014). These results in 2013 and 2014 were less, –10.1% and –3.2 %, respectively, than those determined by the side-by-side comparison with the reference sky-radiometer.

Although the monthly mean calibration constant of the water vapor channel was underestimated every year in the wet season (May to October), it was a good estimate in the dry season (November to April). The number of retrieved results was small in summer because of cloudiness. In summer in Japan, clouds develop every day because it is warm with high relative humidity. Thus, because of higher aerosol optical thickness and as a result of the cloud-affected data, PWV in summer also contained large bias. We rejected the monthly calibration constant, which was calculated from fewer 50 data sets. Figures 12b and 13b show the DSRAD-retrieved PWV, which is denoted by $PWV_{DSRAD+SKYMAP}$, using the monthly calibration constant. $PWV_{DSRAD+SKYMAP}$ of the sky-radiometer agreed well with that of the GNSS/GPS receiver.

https://doi.org/10.5194/amt-2019-426
Preprint. Discussion started: 11 December 2019


Atmospheric Measurement Techniques Discussions

Although monthly mean values are best, in theory, they could not be obtained during the wet season or during periods of high aerosol optical thickness in transported dust. Thus we calculated the annual mean value from all data in a year. Figures 12c and 13c describe PWV using the annual mean value for the year. The retrieved PWV agreed well with PWV from the GNSS/GPS receiver (correlation coefficient γ = 0.987 and 0.987, and slope = 0.919 and 0.934 for 2013 and 2014, respectively). We estimated PWV, which is denoted by $PWV_{DSRAD+LM}$, from the DSRAD algorithm using the calibration constant obtained by the side-by-side comparison with the reference sky-radiometer. The comparison of $PWV_{DSRAD+LM}$ and the GNSS/GPS-derived PWV in Figs. 12d and 13d shows the good agreement, and the results are similar to those in Figs. 12c and 13c. Then we compared $PWV_{DSRAD+LM}$ and $PWV_{DSRAD+SKYMAP}$ in Figs. 12e and 13e. The difference between $PWV_{DSRAD+LM}$ and $PWV_{DSRAD+SKYMAP}$ was small: 17% in 2013, and 8% in 2014. Our self-calibration method showed comparable results to those based on the Langley method.

4.2 Observation at Chiba

We used 2017 data from the sky-radiometer (S/N PS2501417) at Chiba University (35.63°N, 140.10°E). The PWV was also obtained by a Radiometrix MP-1500 microwave radiometer (MWR) and AERONET sun-sky radiometer (Cimel, France) at the same location. The MWR measured in the 22-30 GHz region at 1-min temporal resolution and retrieved PWV_{MWR} using default software. PWV_{Cimel} of the AERONET sun-sky radiometer was retrieved by direct solar irradiance at 940 nm with adjustment parameters (direct sun algorithm version 3; Holben *et al*., 1998; Giles *et al*., 2018) and adopted the cloud screening method (AERONET Level 2.0). The AERONET product comprises three types of data: Level 1.0 data are not screened for cloud-affected or low quality-data, Level 1.5 data are screened but not completely calibrated, and Level 2.0 data are finalized data that have been calibrated and screened. We used PWV for the Level 2.0 data.

Figure 14 shows comparisons of $PWV_{DSRAD+SKYMAP}$ using the monthly and annual means of the calibration constant, PWV_{MWR}, and PWV_{Cimel}. $PWV_{DSRAD+SKYMAP}$ using monthly means agreed well (correlation coefficient γ = 0.961 and slope = 0.964) with those of the MWR (Fig. 14b). $PWV_{DSRAD+SKYMAP}$ using the annual mean calibration constant agreed with PWV_{MWR} within ±0.05 cm for low PWV (<3 cm), but was smaller than PWV_{MWR} for high PWV (Fig. 14c). Figure 14d also shows that $PWV_{DSRAD+SKYMAP}$ using the annual mean calibration constant was smaller than PWV_{Cimel} when PWV was >3 cm. PWV_{MWR} was larger than PWV_{Cimel} (Fig. 14e). $PWV_{DSRAD+SKYMAP}$ using the annual mean calibration constant was smaller than PWV_{MWR} and PWV_{Cimel}, but the difference was 10 % compared to the MWR and 16% compared to the AERONET sun-sky radiometer.

https://doi.org/10.5194/amt-2019-426
Preprint. Discussion started: 11 December 2019

Atmospheric Measurement Techniques Discussions

5 Summary

We developed a new on-site self-calibration method, SKYMAP, to retrieve PWV from sky-radiometer data at the water vapor channel. This method first retrieves PWV from the angular distribution of the normalized radiance without the calibration constant. Then the calibration constant is retrieved from the obtained PWV. Once the calibration constant is determined, PWV can be estimated from the direct solar irradiance. Our DSRAD algorithm retrieves PWV from the direct solar irradiance. This method does not require any of the adjustment parameters used in previous studies (e.g., Holben *et al.*, 1998; Uchiyama *et al.*, 2014). Instead, the filter response function and the vertical profiles of water vapor, temperature, and pressure are required as input parameters.

Sensitivity tests using simulated data from sky-radiometer measurements showed that SKYMAP retrieved PWV within an error of 0.5 cm for cases when PWV was <2 cm. Much more retrieval error occurred, when PWV was >2 cm, because PWV became less sensitive to the angular distribution of the normalized radiance.

We applied SKYMAP and DSRAD algorithms to sky-radiometer measurements at two SKYNET sites (Tsukuba and Chiba, Japan). At Tsukuba, the calibration constant estimated by SKYMAP was compared to that obtained by side-by-side comparison with a sky-radiometer calibrated by the Langley method. Their differences were–10.1% in 2013 and –3.2% in 2014. Our retrieved PWV data were compared to those obtained by a GNSS/GPS receiver, a microwave radiometer, and an AERONET sun-sky radiometer. The correlation coefficients and slopes were as good as >0.96 and 1.00 ± 0.12, respectively. These results show that our new on-site self-calibration method is practical.

.

6 Data availability

The SKYMAP and DSRAD algorithms are available on request from the first author. The sky-radiometer data are available from the SKYNET website (http://www.skynet-isdc.org/), but the sky-radiometer data in Tsukuba, Japan, are available on request from the first author. The MWR data at Chiba University are available from CEReS, Chiba University (http://atmos3.cr.chiba-u.jp/skynet/). The AERONET sun-sky radiometer data are available from the AERONET website (https://aeronet.gsfc.nasa.gov/).

Author contributions

This study was designed by MM, RK, KA, TM, KM, and TN. Sky-radiometer measurements at Tsukuba were conducted by RK. Sky-radiometer and MWR measurements at Chiba were conducted by HO and HI. Analyses of both sky-radiometers were performed by MM. The calibration constant of the

https://doi.org/10.5194/amt-2019-426
Preprint. Discussion started: 11 December 2019

sky-radiometer by the Langley method was provided by AU. Analyses of the GPS receiver were conducted by YS. Visual observations at Tsukuba were conducted by OI and MT. The manuscript was written by MM and RK, and all authors contributed to editing and revision.

Competing interests

The authors declare that they have no conflict of interest.

Acknowledgments

This work was performed by the joint research programs of CEReS, Chiba University (2018), and the Environment Research and Technology Development Fund (S-12) of the Environmental Restoration and Conservation Agency. We are grateful to the OpenCLASTR project (http://157.82.240.167/~clastr/, last accessed September 2018) for allowing us to use SKYRAD.pack (sky-radiometer analysis package), RSTAR (System for Transfer of Atmospheric Radiation for Radiance calculations), and PSTAR (System for Transfer of Atmospheric Radiation for Polarized radiance calculations) in this research. We acknowledge the AERONET networks for providing retrievals. NCEP reanalysis data were provided by the NOAA/OAR/ESRL PSD (Boulder, CO, USA) website at http://www.esrl.noaa.gov/psd/ (last accessed September 2018).

References

Bevis, M., S. Businger, T. A. Herring, C. Rocken, R. A. Anthes, and R. H. Ware, 1992: GPS meteorology: Remote sensing of atmospheric water vapor using the Global Positioning System, *J. Geophys. Res.*, **97**, 15787-15801

Boi, P., G. Tonna, G. Dalu, T. Nakajima, B. Olivieri, A. Pompei, M. Campanelli, and R. Rao, 1999: Calibration and data elaboration procedure for sky irradiance measurements, *Appl. Opt.*, **38**, 6, 896-907

Bruegge, C. J., J. E. Conel, R. O. Green, J. S. Margolis, R. G. Holm and G. Roon, 1992: Water vapor column abundance retrievals during FIFE, *J. Geophys. Res.*, **97**, 18759-18768

Campanelli, M., T. Nakajima and B. Olivieri, 2004: Determination of the solar calibration constant for a sun-sky radiometer: proposal of an in-situ procedure, *Appl. Opt.*, **43**, 651-659

Campanelli, M., V. Estellés, C. Tomasi, T. Nakajima, V. Malvestuto and J. A. Martínez-Lozano, 2007: Application of the SKYRAD Improved Langley plot method for the in situ calibration of CIMEL Sun-sky photometers, *Appl. Opt.*, **46**, 2688-2702

Campanelli, M., T. Nakajima, P. Khatri, T. Takamura, A. Uchiyama, V. Estelles, G. L. Liberti and V. Malvestuto, 2014: Retrieval of characteristic parameters for water vapour transmittance in the

https://doi.org/10.5194/amt-2019-426
Preprint. Discussion started: 11 December 2019

development of ground-based sun-sky radiometric measurements of columnar water vapour, *Atmos. Meas. Tech.*, **7**, 1075-1087

Campanelli, M., A. Mascitelli, P. Sanò, H. Diémoz, V. Estellés, S. Federico, A. M. Iannarelli, F. Fratarcangeli, A. Mazzoni, E. Realini, M. Crespi, O. Bock, J. A. Martínez-Lozano and S. Dietrich, 2018: Precipitable water vapour content from ESR/SKYNET sun–sky radiometers: validation against GNSS/GPS and AERONET over three different sites in Europe, *Atmos. Meas. Tech.*, **11**, 81-94

Dubovik, O., A. Smirnov, B. N. Holben, M. D. King, Y. J. Kaufman, T. F. Eck, and I. Slutsker, 2000: Accuracy assessments of aerosol optical properties retrieved from Aerosol Robotic Network (AERONET) Sun and sky radiance measurements, *J. Geophys. Res.*, **105**, 9791–9806

Dubovik, O. and M. D. King, 2000: A flexible inversion algorithm for retrieval of aerosol optical properties from sun and sky radiance measurements, *J. Geophys. Res.*, **105**, 20673–20696

Dubovik, O., A. Sinyuk, T. Lapyonok, B. N. Holben, M. Mishchenko, P. Yang, T. F. Eck, H. Volte, O. Muñoz, B. Veihelmann, W. J. van der Zande, J.-F. Leon, M. Sorokin, and I. Slutsker, 2006: Application of spheroid models to account for aerosol particle nonsphericity in remote sensing of desert dust, *J. Geophys. Res.*, **111**, D11208, doi:10.1029/2005JD006619

Estellés, V., M. Campanelli, M. P. Utrillas, F. Expósito, and J. A. Martínez-Lozano, 2012: Comparison of AERONET and SKYRAD4.2 inversion products retrieved from a Cimel CE318 sunphotometer, *Atmos. Meas. Tech.*, **5**, 569-579, doi:10.5194/amt-5-569-2012

Fowle, F. E., 1912: The spectroscopic determination of aqueous vapor, *Astrophys. J.*, **35**, 149-162

Fowle, F. E., 1915: The transparency of aqueous vapor, *Astrophys. J.*, **42**, 394-411

Fröhlich, C. and Shaw, G. E., 1980: New determination of Rayleigh scattering in the terrestrial atmosphere, *Appl. Opt.*, **19**, 1.773– 1.775

Giles, D. M., A. Sinyuk, M. G. Sorokin, J. S. Schafer, A. Smirnov, I. Slutsker, T. F. Eck, B. N. Holben, J. R. Lewis, J. R. Campbell, E. J. Welton, S. V. Korkin, and A. I. Lyapustin, 2019: Advancements in the Aerosol Robotic Network (AERONET) Version 3 database – automated near-real-time quality control algorithm with improved cloud screening for Sun photometer aerosol optical depth (AOD) measurements, *Atmos. Meas. Tech.*, **12**, 169-209, https://doi.org/10.5194/amt-12-169-2019

Gueymard, C. A., 2001: Parameterized transmittance model for direct beam and circumsolar spectral irradiance, *Solar Energy*, **71**, 325-346

Halthore, R. N., T. F. Eck, B. N. Holben and B. L. Markham, 1997: Sun photometric measurements of atmospheric water vapor column abundance in the 940-nm band, *J. Geophys. Res.*, **102**, 4343-4352

Hashimoto, M., T. Nakajima, O. Dubovik, M. Campanelli, H. Che, P. Khatri, T. Takamura, and G. Pandithurai, 2012: Development of a new data-processing method for SKYNET sky radiometer observations, *Atmos. Meas. Tech.*, **5**, 2723-2737

Hess, M., P. Koepke, and I. Schult, 1999: Optical properties of aerosols and clouds: the software package OPAC, *B. Am. Meteorol. Soc.*, **79**, 831–844

https://doi.org/10.5194/amt-2019-426
Preprint. Discussion started: 11 December 2019

Atmospheric Measurement Techniques Discussions

Holben, B. N., T. F. Eck, I. Slutsker, D. Tanré, J. P. Buis, A. Setzer, E. Vermote, J. A. Reagan, Y. J. Kaufman, T. Nakajima, F. Lavenu, I. Jankowiak and A. Smirnov, 1998: AERONET-A federated instrument network and data archive for aerosol characterization, *Remote Sens. Environ.*, **66**, 1-16

IPCC, Summary for Policymakers. In: Climate Change 2013: The Physical Science Basis. 5 Contribution of Working Group I to the Fifth Assessment Report of the Intergovernmental 6 Panel on Climate Change [Stocker, T.F., D. Qin, G.-K. Plattner, M. Tignor, S.K. Allen, J. 7 Boschung, A. Nauels, Y. Xia, V. Bex and P.M. Midgley (eds.)], Cambridge University Press, 8 Cambridge, United Kingdom and New York, NY, USA., 2013

Kasten, F. and A. T. Young, 1989: Revised optical air mass tables and approximation formula, *Appl. Opt.*, **28**, 4735-4738

Kudo, R., T. Nishizawa, and T. Aoyagi, 2016: Vertical profiles of aerosol optical properties and the solar heating rate estimated by combining sky radiometer and lidar measurements, *Atmos. Meas. Tech.*, **9**, 3223–3243, doi:10.5194/amt-9-3223-2016

Nagasawa, K. 1999: Computations of Sunrise and Sunset, Chijin-Shoin (in Japanese)

Nakajima, T., and M. Tanaka, 1986: Matrix formulations for the transfer of solar radiation in a plane-parallel scattering atmosphere. *J. Quant. Spectrosc. Radiat. Transfer*, **35**, 13–21

Nakajima, T., and M. Tanaka, 1988: Algorithms for radiative intensity calculations in moderately thick atmospheres using a truncation approximation. *J. Quant. Spectrosc. Radiat. Transfer*, **40**, 51–69

Nakajima, T., G. Tonna, R. Rao, P. Boi, Y. Kaufman and B. Holben, 1996: Use of Sky brightness measurements from ground for remote sensing of particulate polydispersions, *Appl. Opt.*, **35**, 2672-2686

Nakajima, T., S. C. Yoon, V. Ramanathan, G. Y. Shi, T. Takemura, A. Higurashi, T. Takamura, K. Aoki, B. J. Sohn, S. W. Kim, H. Tsuruta, N. Sugimoto, A. Shimizu, H. Tanimoto, Y. Sawa, N. H. Lin, C. T. Lee, D. Goto, and N. Schutgens, 2007: Overview of the atmospheric brown cloud east Asia regional experiment 2005 and a study of the aerosol direct radiative forcing in east Asia, *J. Geophys. Res.*, **112**, D24S91, doi:10.1029/2007JD009009

Kneizys, F. X., E. P. Shettle, L. W. Abreu, J. H. Chetwynd, G. P. Anderson, W. O. Gallery, J. E. A. Selby, and S. A. Clough, 1988: Users guide to LOWTRAN-7, AFGL-TR-88-0177, NTIS ADA206773, Air Force Geophysics Laboratory, Hanscom Air Force Base, MA

Kobayashi, E., A. Uchiyama, A. Yamazaki, and K. Matsuse, 2006: Application of the Statistical Optimization Method to the Inversion Algorithm for Analyzing Aerosol Optical Properties from Sun and Sky Radiance Measurements, *J. Meteor. Soc. Japan*, **84**, 1047-1062

Ota, Y., A. Higurashi, T. Nakajima, and T. Yokota, 2010: Matrix formulations of radiative transfer including the polarization effect in a coupled atmosphere–ocean system. *J. Quant. Spectrosc. Radiat. Transfer*, **111**, 878–894

https://doi.org/10.5194/amt-2019-426
Preprint. Discussion started: 11 December 2019

Atmospheric Measurement Techniques Discussions

Schmid, B., K. J. Thome, P. Demoulin, R. Peter, C. Matzler and J. Sekler, 1996: Comparison of modeled and empirical approaches for retrieving columnar water vapor from solar transmittance measurements in the 0.94-mm region, *J. Geophys. Res.*, **101**, 9345-9358

Schmid, B., J. J. Michalsky, D. W. Slater, J. C. Barnard, R. N. Halthore, J. C. Liljegren, B. N. Holben, T. F. Eck, J. M. Livingston, P. B. Russell, T. Ingold and I. Slutsker, 2001: Comparison of columnar water-vapor measurements from solar transmittance methods, *Appl. Opt.*, **40**, 1886-1896

Sekiguchi, M., and T. Nakajima, 2008: A k-distribution- based radiation code and its computational optimization for an atmospheric general circulation model, *J. Quant. Spectrosc. Radiat. Transfer*, **109**, 2779 –2793

Shoji, Y., 2013: Retrieval of Water Vapor Inhomogeneity Using the Japanese Nationwide GPS Array and its Potential for Prediction of Convective Precipitation, *J. Meteor. Soc. Japan*, **91**, 43-62

Smirnov, A., B. N. Holben, T. F. Eck, O. Dubovik, and I. Slutsker, 2000: Cloud-Screening and Quality Control Algorithms for the AERONET Database, *Remote Sens. Environ.*, **73**, 337-349

Takamura, T. and T. Nakajima, 2004: Overview of SKYNET and its activities, *Proceedings of AERONET workshop. EL Arenosillo. Opt. Pura y Apl.*, **37**, 3303-3308

Tanaka, M., T. Nakajima, and M. Shiobara, 1986: Calibration of a sunphotometer by simultaneous measurements of direct-solar and circumsolar radiances, *Appl. Opt.*, **25**, 1170-1176

Torres, B., O. Duvobik, C. Toledano, A. Berjon, V. E. Cachorro, T. Lapyonok, P. Litvinov, and P. Goloub, 2014: Sensitivity of aerosol retrieval to geometrical configuration of ground-based sun/sky radiometer observation, *Atmos. Chem. Phys.*, **14**, 847-875

Twomey, S.A., 1990: Aerosol cloud physics and radiation, in *Seventh Conf. on Atm. Rad.*, AMS, San Francisco, CA, pp. j25-j28

Uchiyama, A., A. Yamazaki and R. Kudo, 2014: Column Water Vapor Retrievals from Sky Radiometer (POM-02) 940 nm Data, *J. Meteor. Soc. Japan*, **92A**, 195-203

Uchiyama A., T. Matsunaga, and A. Yamazaki, 2018a: The instrument constant of sky radiometers (POM-02) – Part 1: Calibration constant, *Atmos. Meas. Tech.*, **11**, 5363-5388

Uchiyama A., T. Matsunaga, and A. Yamazaki, 2018b: The instrument constant of sky radiometers (POM-02) – Part 2: Solid view angle, *Atmos. Meas. Tech.*, **11**, 5389-5402

https://doi.org/10.5194/amt-2019-426
Preprint. Discussion started: 11 December 2019

Atmospheric Measurement Techniques Discussions

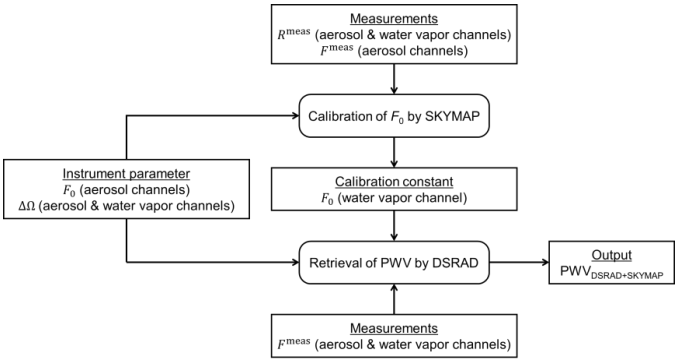

Figure 1: Diagram of the on-site self-calibration method (SKYMAP) and retrieval of PWV from direct solar irradiances (DSRAD).

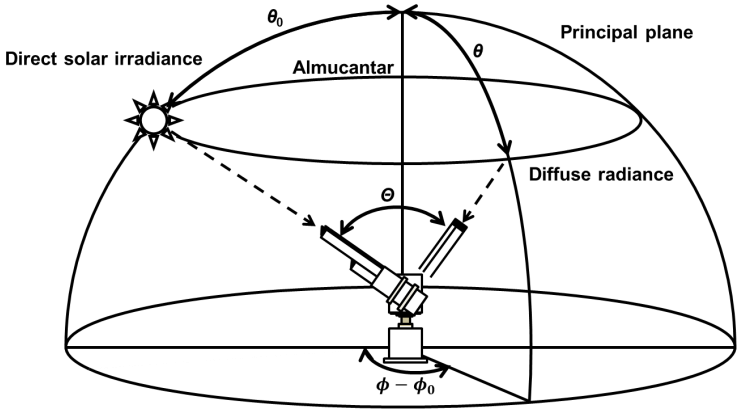

Figure 2: Observation planes (almucantar and principal planes) of the sky-radiometer.

https://doi.org/10.5194/amt-2019-426
Preprint. Discussion started: 11 December 2019

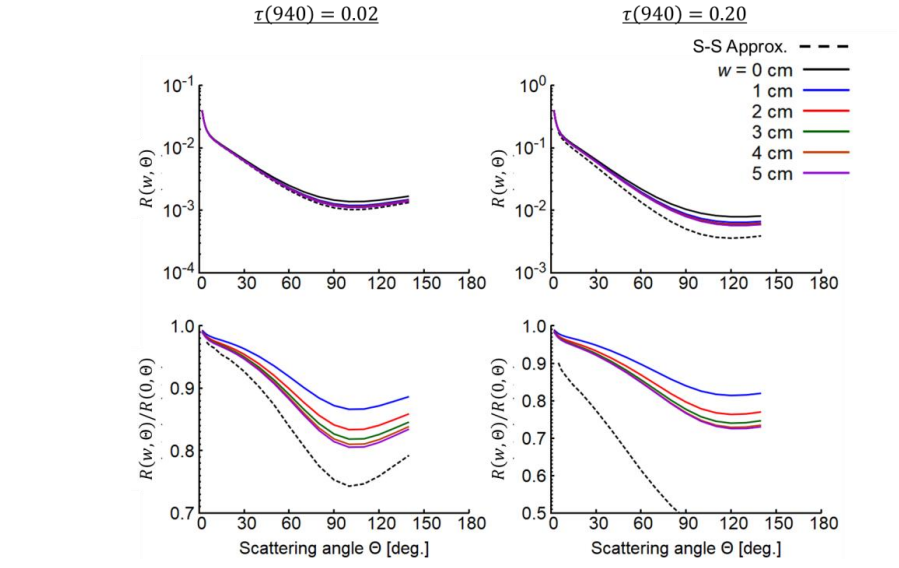

Figure 3: Normalized angular distributions simulated for continental average aerosol (Table 1) at aerosol optical thicknesses of 0.02 and 0.20 at 940 nm. The simulations were conducted for SZA = 70° and PWV (w) = 0, 1, 2, 3, 4, and 5 cm. The top line is the normalized radiance $R(w, \Theta)$, and the bottom line is the ratio of $R(w, \Theta)$ to $R(0, \Theta)$.

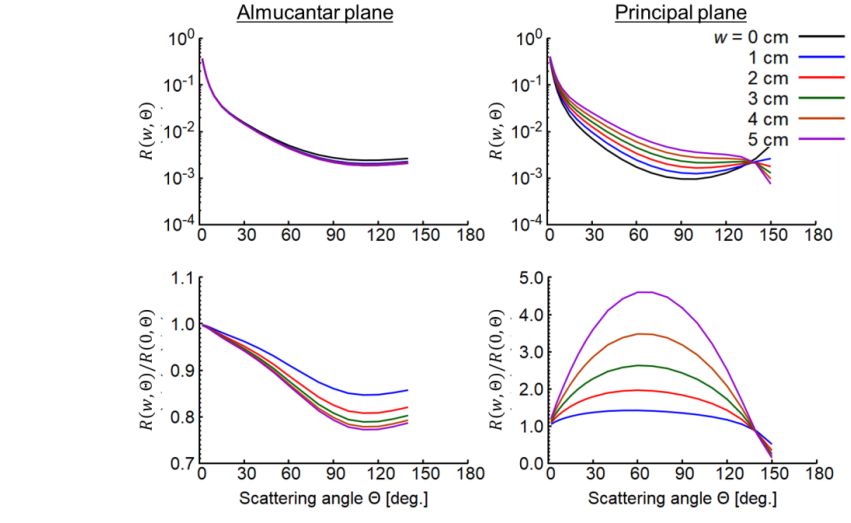

Figure 4: Normalized angular distributions simulated for transported dust aerosol (Table 1) in the almucantar and principal planes at an aerosol optical thickness of 0.06 at 940 nm. The simulations were conducted for SZA = 70° and PWV (w) = 0, 1, 2, 3, 4, and 5 cm. The top line is the normalized radiance $R(w, \Theta)$, and the bottom line is the ratio of $R(w, \Theta)$ to $R(0, \Theta)$.

https://doi.org/10.5194/amt-2019-426
Preprint. Discussion started: 11 December 2019

Atmospheric Measurement Techniques Discussions

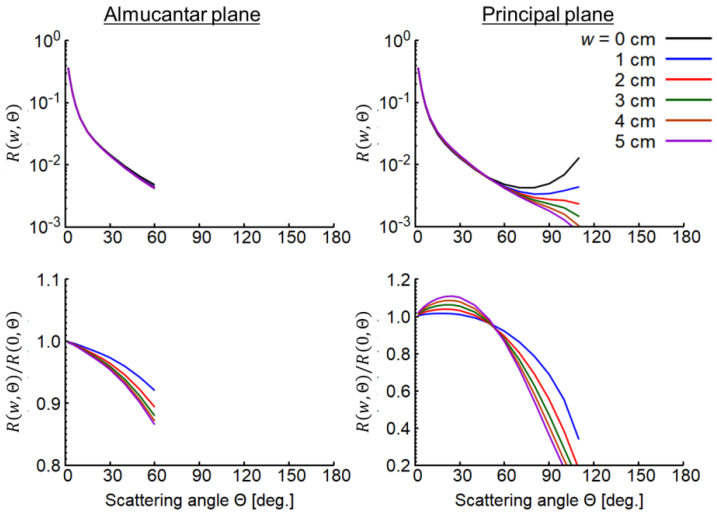

695 **Figure 5: Similar to Fig. 4 but for SZA = 30°.**

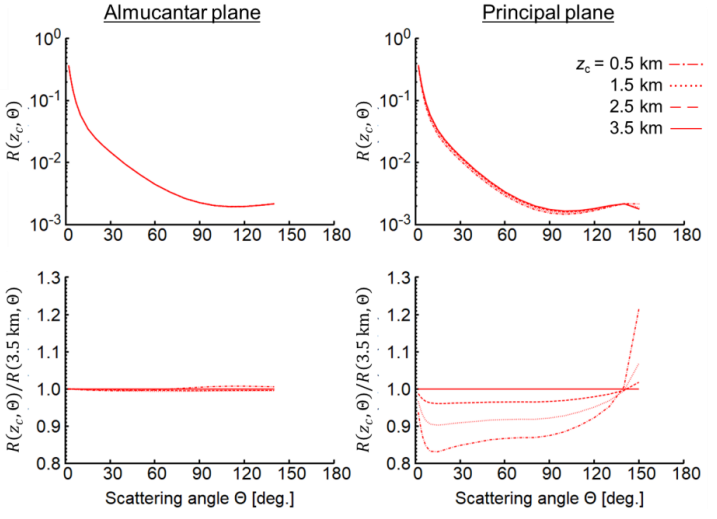

700 **Figure 6: Normalized angular distributions simulated for transported dust aerosol (Table 1) in the almucantar and principal planes at an aerosol optical thickness of 0.06 at 940 nm. The simulations were conducted for SZA = 70° and PWV = 2 cm. The height of the dust layer (z_c) is changed to 0.5, 1.5, 2.5, and 3.5 km. The top line is the normalized radiance $R(z_c, \Theta)$, and the bottom line is the ratio of $R(z_c, \Theta)$ to $R(3.5\ \mathrm{km}, \Theta)$.**

https://doi.org/10.5194/amt-2019-426
Preprint. Discussion started: 11 December 2019

Atmospheric Measurement Techniques Discussions

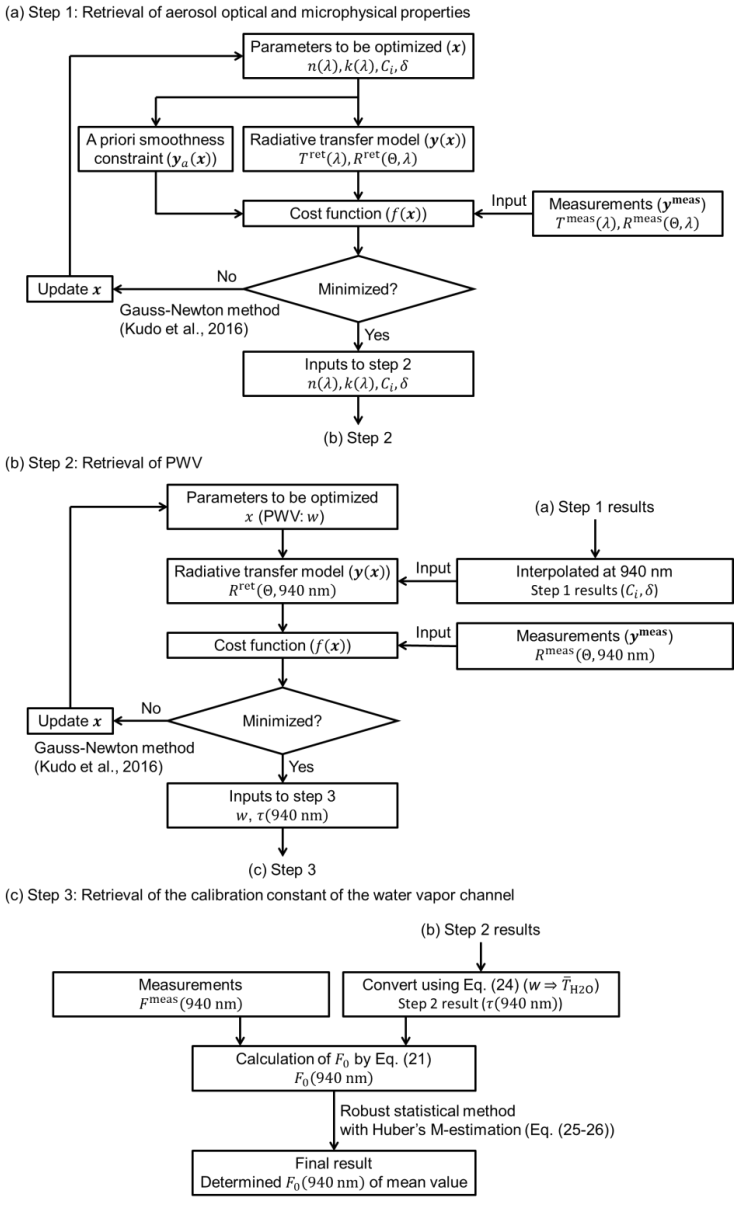

705

Figure 7: Schematic diagrams of SKYMAP procedures. (a) Step 1. (b) Step 2. (c) Step 3.

https://doi.org/10.5194/amt-2019-426
Preprint. Discussion started: 11 December 2019

Atmospheric Measurement Techniques Discussions

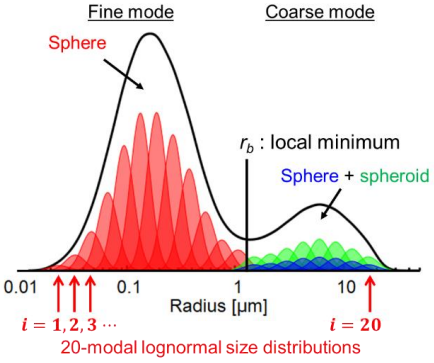

Figure 8: Assuming volume size distributions in the SKYMAP algorithm. Fine and coarse mode particles are separated at radius r_b. Spheroid particles are assumed only in coarse mode. The black line is the volume size distribution, which is computed by the integration of 20-modal lognormal functions (red, blue, and green lines).

https://doi.org/10.5194/amt-2019-426
Preprint. Discussion started: 11 December 2019

Atmospheric Measurement Techniques Discussions

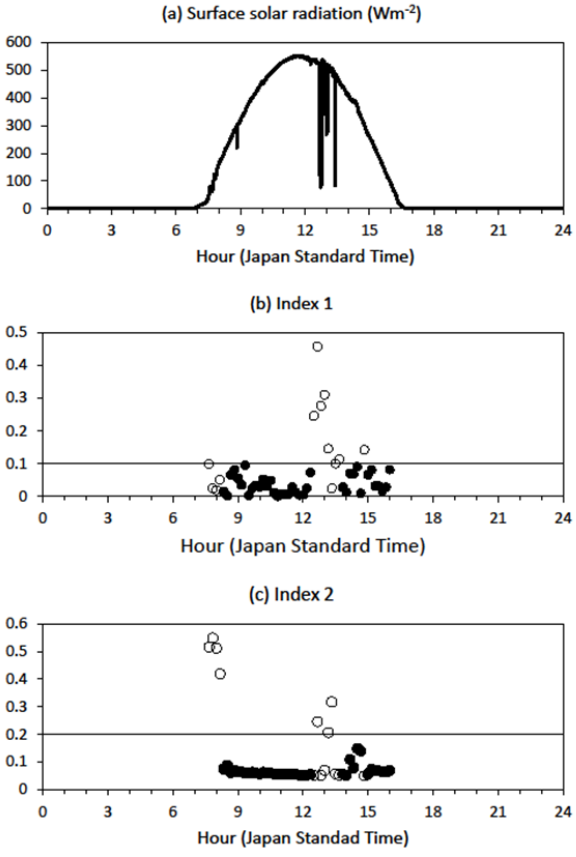

Figure 9: An example result of the SCAD method on January 6, 2014, in Tsukuba. (a) Surface solar radiation observed by the pyranometer. (b) Index 1. (c) Index 2. The closed circles indicate clear-sky conditions and the open circles indicate cloudy conditions in (b) and (c). The lines at 0.1 in (b) and 0.2 in (c) are thresholds for indexes 1 and 2, respectively.

https://doi.org/10.5194/amt-2019-426
Preprint. Discussion started: 11 December 2019

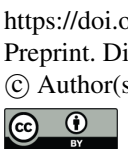

Atmospheric Measurement Techniques Discussions

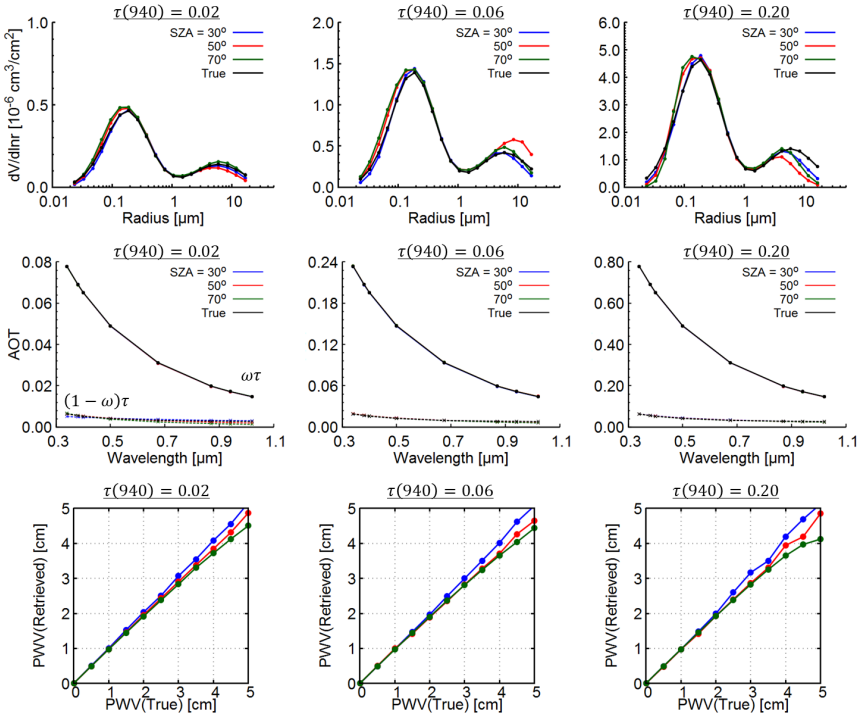

Figure 10: Retrieval results from simulated data for continental average aerosol. The top line is the volume size distribution, the middle line is the scattering and absorption parts of aerosol optical thickness, and the bottom line is a comparison of the "true" and retrieval values of PWV. Blue, red, and green lines are the retrieval results at SZA = 30°, 50°, and 70°, respectively. The black line is the "true" value.

https://doi.org/10.5194/amt-2019-426
Preprint. Discussion started: 11 December 2019

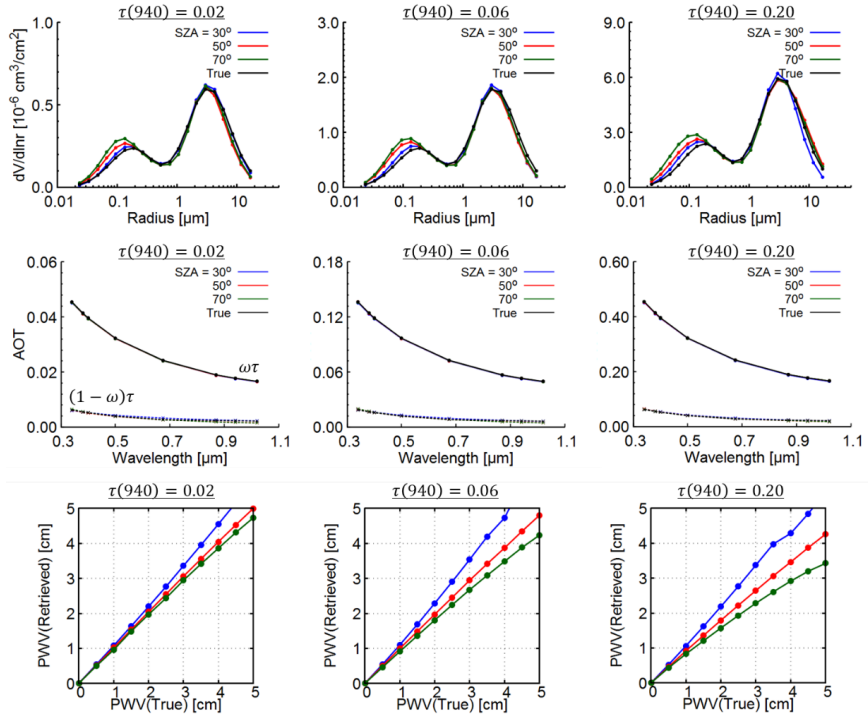

Figure 11: Similar to Fig. 10 but for transported dust aerosol.

https://doi.org/10.5194/amt-2019-426
Preprint. Discussion started: 11 December 2019

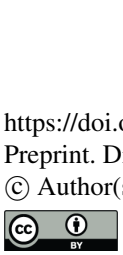

Atmospheric Measurement Techniques Discussions

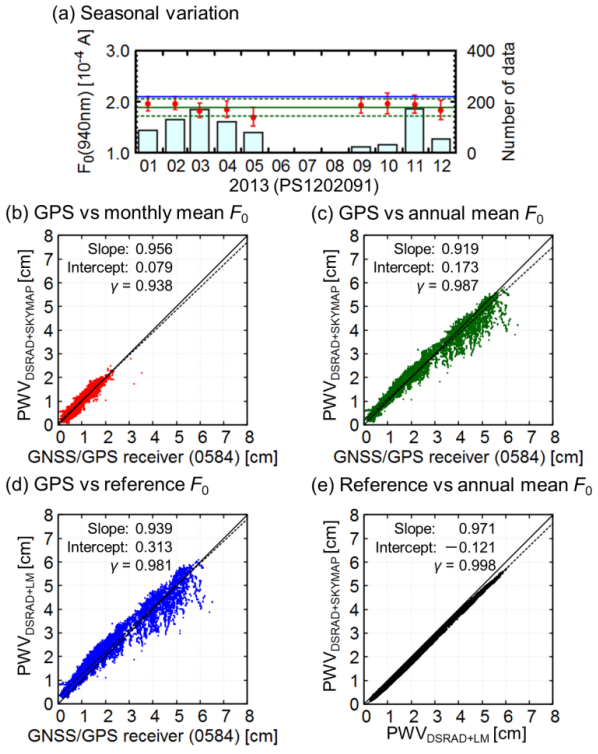

Figure 12: Application of our methods to observational data from Tsukuba in 2013. (a) Seasonal variation in the calibration constant of the water vapor channel (red circles and error bars are monthly means and standard deviations, respectively; green solid and dotted lines are annual means and standard deviations, respectively; the blue line is the value obtained by a side-by-side comparison with the reference sky-radiometer; boxes indicate the number of data points). (b-d) Comparisons of PWV between the GNSS/GPS receiver and the sky-radiometer with (b) the monthly mean F_0, (c) the annual mean F_0, and (d) the reference F_0. (e) Comparison of PWV from the sky-radiometer with the reference and annual mean F_0.

https://doi.org/10.5194/amt-2019-426
Preprint. Discussion started: 11 December 2019

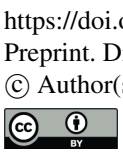

Atmospheric Measurement Techniques Discussions

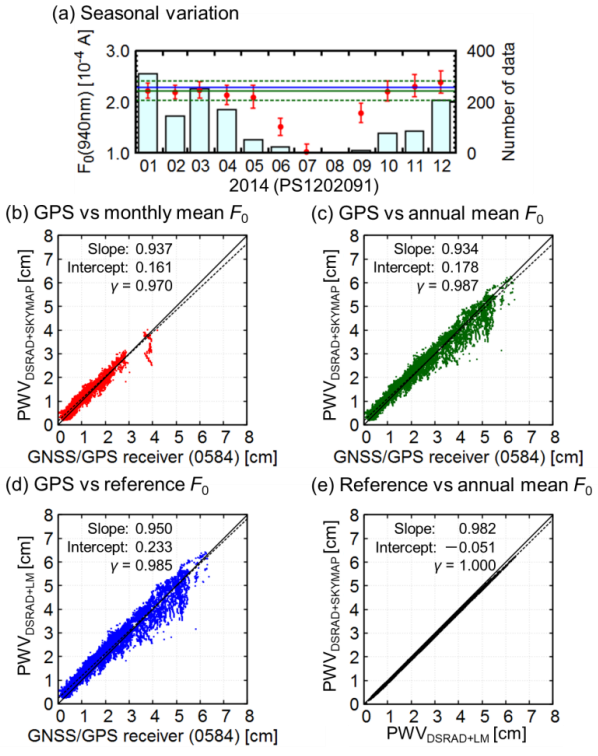

745

Figure 13: Similar to Fig. 12 but in 2014.

https://doi.org/10.5194/amt-2019-426
Preprint. Discussion started: 11 December 2019

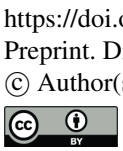

Atmospheric Measurement Techniques Discussions

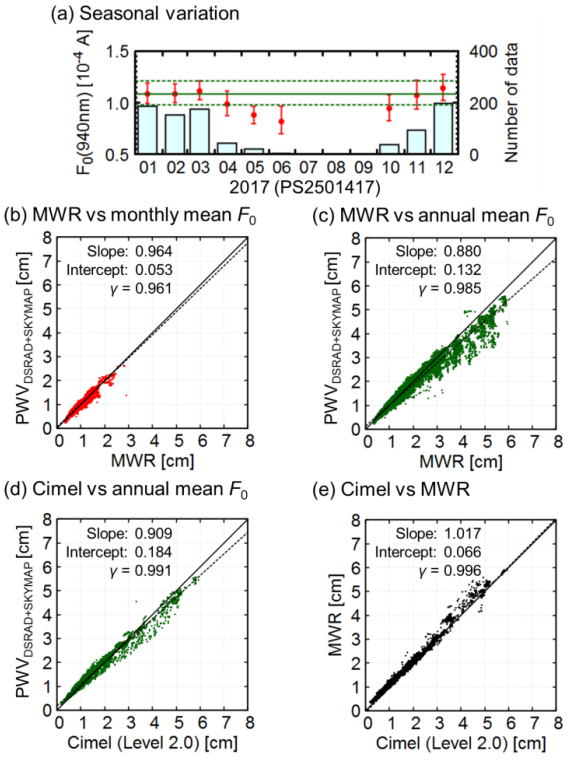

Figure 14: Application of our methods to observational data from Chiba in 2017. (a) Seasonal variation in the calibration constant of the water vapor channel (red circles and error bars are monthly means and standard deviations, respectively; green solid and dotted lines are annual means and standard deviations, respectively; boxes indicate the number of data points). (b-c) Comparison of PWV between the MWR and the sky-radiometer with (b) the monthly mean F_0, (c) the annual mean F_0. (d) Comparison of PWV between the Cimel level 2.0 data and the sky-radiometer with annual mean F_0. (e) Comparison of PWV between the Cimel level 2.0 data and the MWR.

https://doi.org/10.5194/amt-2019-426
Preprint. Discussion started: 11 December 2019

Atmospheric Measurement Techniques Discussions

Table 1: Microphysical and optical properties and vertical profiles of aerosol used in sensitivity tests.

Aerosol	Components	Particle shape	Size distribution		Refractive index at 940 nm		Relative weight in total optical thickness at 500 nm	Vertical profile
			Mode radius (μm)	Mode width	Real	Imaginary		
Continental average	Water-soluble	Sphere	0.18	0.81	1.43	0.0074	0.90	$\exp(-z/H)$, $H = 8$ km
	Soot	Sphere	0.05	0.69	1.75	0.44	0.07	$\exp(-z/H)$, $H = 4$ km
	Insoluble	Spheroid	5.98	0.92	1.52	0.008	0.03	$\exp(-z/H)$, $H = 2$ km
Transported dust	Dust	Spheroid	3.23	0.79	1.53	0.004	0.25	$\frac{1}{\sqrt{2\pi}\sigma}\exp\left(-\frac{(z-z_c)}{2\sigma^2}\right)$, $z_c = 3.5$ km $\sigma = 0.4$ km
	Water-soluble	Sphere	0.18	0.81	1.43	0.0074	0.67	$\exp(-z/H)$, $H = 8$ km
	Soot	Sphere	0.05	0.69	1.75	0.44	0.05	$\exp(-z/H)$, $H = 4$ km
	Insoluble	Spheroid	5.98	0.92	1.52	0.008	0.03	$\exp(-z/H)$, $H = 2$ km

Table 2: Validation of the SCAD method by visual observation from 2013 to 2014 in Tsukuba.

Visual observation	Sky-radiometer measuring plane	
Cloud cover	Clear sky	Cloud affected
Clear, less than 1	**463 (83.4%)***	68 (9.3%)
Cloud affected, more than 2	**92 (16.6%)†**	**663(90.7%)***

*Obviously correct determination.

†Obviously incorrect determination.

Table 3: References and methodologies of the DSRAD algorithm.

	DSRAD
Solar coordinates	Nagasawa (1999)
Refraction correction	Nagasawa (1999)
Sun-Earth distance	Nagasawa (1999)
Optical mass	Gueymard (2001)
Rayleigh scattering	Fröhlich and Shaw (1980); Young(1981)
Ozone absorption	Correlated *k*-distribution
Water vapor absorption	Correlated *k*-distribution
Filter response function	Stepwise function
Retrieved the PWV	Newton-Raphson method